

# Finite element analysis for laterally loaded piles in sloping ground

Vishwas A. Sawant\*<sup>1</sup> and Sanjay Kumar Shukla<sup>2</sup>

<sup>1</sup>*Department of Civil Engineering, Indian Institute of Technology, Roorkee, India*

<sup>2</sup>*Discipline of Civil Engineering, School of Engineering, Edith Cowan University, Perth, WA 6027, Australia*

*(Received February 9, 2012, Revised March 5, 2012, Accepted March 8, 2012)*

**Abstract.** The available analytical methods of analysis for laterally loaded piles in level ground cannot be directly applied to such piles in sloping ground. With the commercially available software, the simulation of the appropriate field condition is a challenging task, and the results are subjective. Therefore, it becomes essential to understand the process of development of a user-framed numerical formulation, which may be used easily as per the specific site conditions without depending on other indirect methods of analysis as well as on the software. In the present study, a detailed three-dimensional finite element formulation is presented for the analysis of laterally loaded piles in sloping ground developing the 18 node triangular prism elements. An application of the numerical formulation has been illustrated for the pile located at the crest of the slope and for the pile located at some edge distance from the crest. The specific examples show that at any given depth, the displacement and bending moment increase with an increase in slope of the ground, whereas they decrease with increasing edge distance.

**Keywords:** finite element analysis; lateral load; pile; sloping ground; edge distance

---

## 1. Introduction

Many high-rise buildings, transmission towers, and bridges are constructed near slopes and are supported by pile foundations. These structures are exposed to considerable amount of lateral load due to environmental actions, which is ultimately transferred to the pile foundations. The analysis of laterally loaded pile embedded in the level ground has received considerable attention over the past several decades (Reese and Matlock 1956, Matlock and Reese 1960, Davisson and Gill 1963, Matlock 1970, Poulos 1971, Reese and Welch 1975, Randolph 1981, Norris 1986, Budhu and Davies 1988, Prakash and Kumar 1996, Ashour *et al.* 1998, Fan and Long 2005, Basu *et al.* 2009, Zhang 2009, Dewaikar *et al.* 2011).

However, some developments towards the analysis of piles in sloping ground have been made recently either by conducting experiments in laboratory (Mezazigh and Levacher 1998, Muthukkumaran *et al.* 2004) or by performing numerical analysis, mainly based on available commercial software (Gabr and Borden 1990, Chae *et al.* 2004). Several investigators have considered the equivalent problem

---

\* Corresponding author, Assistant Professor, E-mail: [sawntfce@gmail.com](mailto:sawntfce@gmail.com)

of battered piles in horizontal ground. For example, Zhang *et al.* (1999) performed centrifuge tests of battered piles in sand and proposed reduction or increase in the ultimate load  $p_u$  of the  $p$ - $y$  curves, based on loading direction, batter angle, and soil density.

Brown and Shie (1991) described the results of several numerical experiments performed with a three dimensional finite element model of a laterally loaded pile in clayey slope. The experiments were used to derive the  $p$ - $y$  curves from the model. Results indicate that ground inclination significantly affects ultimate load  $p_u$ , especially close to the ground surface, but has essentially no effect on initial slope of the  $p$ - $y$  curves. Mezazigh and Levacher (1998) carried out an experimental investigation of the behaviour of laterally loaded piles to study the effect of a slope on the  $p$ - $y$  curves in dry sandy soil. The results show that the limiting distance beyond which the slope has no more influence is approximately  $8B$  for a slope of 1 vertical (V) to 2 horizontal (H) and  $12B$  for a slope of 2V to 3H. These values are practically independent of the shear strength of the sand mass. An upper bound plasticity solution for the undrained lateral bearing capacity of piles in sloping clay has been presented by Stewart (1999), who gave charts with reduction factors which are applied to the lateral capacity of piles in level ground. Charles and Zhang (2001) investigated the performance of the sleeved and unsleeved piles constructed on a cut slope using 3D finite difference analysis. The results show that the load transfer of sleeved piles is primarily through a downward shear transfer mechanism in the vertical plane. Chae *et al.* (2004) described the results of several numerical studies performed with a 3D FE model test and prototype test on laterally loaded short rigid piles and pier foundation located near slope. Muthukkumaran *et al.* (2004) conducted an experimental investigation on a single pile to understand effect of lateral movement of unstable slope on pile supported structures. A comparison between the test results conducted in both sloping and horizontal ground has been presented to highlight the effect of sloping ground due to the lateral soil movement. Martin and Chen (2005) evaluated the response of piles caused by an embankment slope, induced by a weak soil layer or a liquefied layer beneath the embankment using FLAC3D program. Begum and Muthukkumaran (2008) presented a two-dimensional finite element analysis of a long flexible pile subjected to a lateral load, located on a sloping ground in cohesionless soil. Piles were represented by an equivalent plate element subjected to plane strain analysis and the soil strata are represented by 15 node triangular elements of elastic-plastic Mohr Coulomb model. The maximum bending moment in the pile was increased by 29% for  $L/D$  ratio of 25 at a slope of 1V:2H with respect to level ground case. Georgiadis and Georgiadis (2010) performed three-dimensional finite element analysis to study the behavior of piles in sloping ground under undrained lateral loading condition. Based on the results, a new  $p$ - $y$  criterion for static loading of piles in clay were proposed which takes into account the inclination of the slope and adhesion of the pile slope interface.

Available information concerning the lateral behaviour of piles in sloping ground is rather limited and mainly refers to piles in cohesionless soil. The available methods of analysis for laterally loaded piles in level ground cannot be directly applied to the laterally loaded piles in sloping ground. The field test is the best option for investigating the pile response for varying slope angles, but it is not cost-effective. Even though scaling effects influence the results of the model test study, it can be an alternative to the field test, but it is inconvenient with varying angles of slopes, as the research works reported in the past. The computer simulation of numerical model can be an economical way to analyze the pile - soil interaction of laterally loaded piles in sloping ground. The simulation of the appropriate field condition is also a challenging task while using the commercially available software. The results are also sensitive to the user defined specifications because of the lack of specific guidelines in the manual of the software. Therefore, it becomes essential to understand the process

of fundamental development of a user-framed numerical formulation, which has several advantages. The developed formulation can be modified easily to suit specific field conditions as per the requirements of the site. Additionally heterogeneity and anisotropy of the soil media can be easily accounted for. In the present study, a detailed three-dimensional finite element formulation is presented for the analysis of laterally loaded pile in sloping ground using the developed 18 node triangular prism elements.

## 2. Problem definition

The subgrade reaction approach and elastic continuum approach are widely used for the analysis of laterally loaded pile embedded in the level ground due to their simplicity. But these approaches cannot be extended directly for the piles in sloping ground. Due to the limitation of these methods for the analysis of piles in sloping ground, the three-dimensional finite element analysis is the only realistic option to predict the load-deflection behaviour of laterally loaded piles. The finite element (FE) modelling approach provides a more precise tool that is capable of modelling soil continuity, pile-soil interface behaviour, and 3-dimensional (3D) boundary conditions (Desai and Appel 1976, Randolph 1981). Fig. 1 shows a schematic diagram of a laterally loaded pile of length  $L$ , embedded completely in a sloping ground inclined to the horizontal for two locations of piles. The pile is subjected to a lateral load  $F_x$  at the pile top along the  $X$ -direction. The  $Z$ -axis is vertical parallel to the pile axis, and the  $X$ - $Y$  defines a horizontal plane. For the sake of convenience in three-dimensional finite element

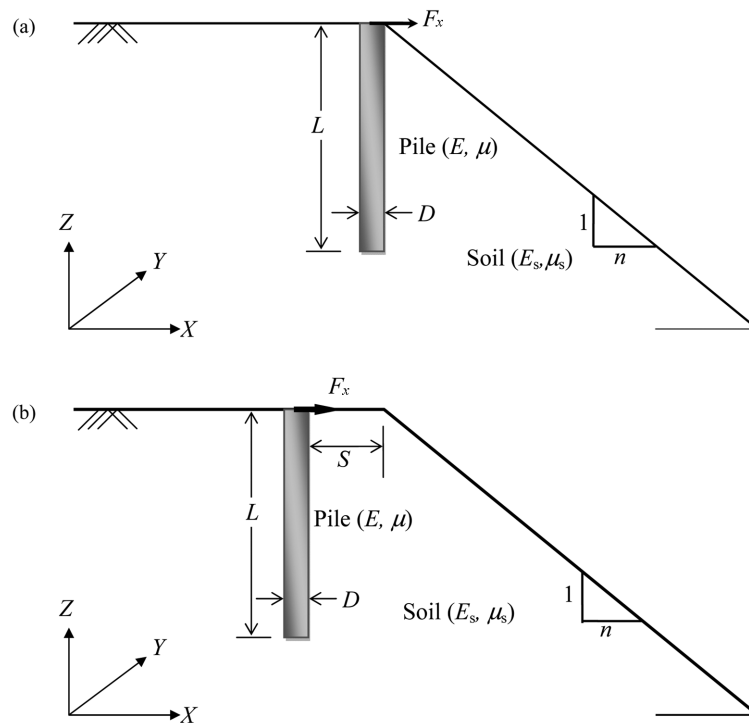


Fig. 1 Schematic diagram of a laterally loaded pile in sloping ground: (a) pile at crest and (b) pile at edge distance,  $S$

(3D FE) mesh generation, the cross-section of the pile has been considered a square of side  $D$ . An attempt has been made to develop the finite element formulation to determine the displacement and the bending moment along the pile length.

### 3. Finite element formulation

#### 3.1 Discretisation of the pile and soil system

The pile and soil system is idealized as an assemblage of 18 node triangular prism continuum elements (Fig. 2). These elements are suitable for modelling the ground slope as well as the response of a system dominated by bending deformations. Each node of the element has three translational degrees of freedom,  $u$ ,  $v$  and  $w$ , in the  $X$ ,  $Y$  and  $Z$  coordinate directions, respectively. Fixing boundaries are assumed at the distance of  $10D$  from edge/tip of the pile in  $X$ ,  $Y$  and  $Z$  directions except at the sloping surface. Sloping ground is considered as a free surface from the pile to its intersection with a horizontal plane  $10D$  below the pile tip. Taking an advantage of the symmetry, only half of the actual domain was built, thus dramatically improving efficiency of computation. The mesh size selected for a finite element solution has been optimized for both accuracy and computational economy based on the analyses of several meshes with different numbers of elements and mesh sizes. The relations used in the formulation are outlined below.

#### 3.2 Displacement model and shape functions

The shape functions which describe the relation between the displacements at any point within the 18 node triangular prism element (Fig. 2) are derived considering quadratic variation in triangular  $XZ$  plane and along  $Y$ -direction. Any point  $P$  is defined in  $XZ$  plane with the set of natural coordinates ( $L_1, L_2, L_3$ ) as:  $L_1 = A_1/A_t$ ;  $L_2 = A_2/A_t$ ;  $L_3 = A_3/A_t$ , where  $A_1, A_2$ , and  $A_3$  are the areas of the three subtriangles, subtended by the point  $P$  and  $A_t$  is total area of triangle. The quadratic

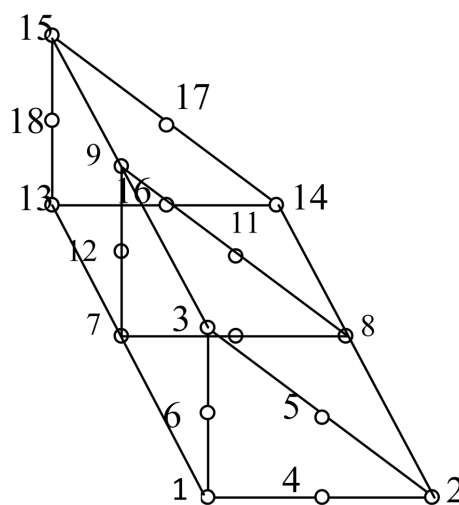


Fig. 2 18 node triangular prism element

variation of displacements in a six node triangular plane ( $XZ$  plane) can be expressed by

$$u = \alpha_1 L_1^2 + \alpha_2 L_2^2 + \alpha_3 L_3^2 + \alpha_4 L_1 L_2 + \alpha_5 L_2 L_3 + \alpha_6 L_3 L_1 \quad (1)$$

In the matrix notation, Eq. (1) can be transformed as

$$\begin{aligned} u &= [L_1^2 \ L_2^2 \ L_3^2 \ L_1 L_2 \ L_2 L_3 \ L_3 L_1] \{\alpha\} \\ \{\alpha\}^T &= [\alpha_1 \ \alpha_2 \ \alpha_3 \ \alpha_4 \ \alpha_5 \ \alpha_6] \end{aligned} \quad (2)$$

From the geometry of the element (Fig. 2)

$$\begin{Bmatrix} u_1 \\ u_2 \\ u_3 \\ u_4 \\ u_5 \\ u_6 \end{Bmatrix} = \begin{bmatrix} 1 & 0 & 0 & 0 & 0 & 0 \\ 0 & 1 & 0 & 0 & 0 & 0 \\ 0 & 0 & 1 & 0 & 0 & 0 \\ 0.25 & 0.25 & 0 & 0.25 & 0 & 0 \\ 0 & 0.25 & 0.25 & 0 & 0.25 & 0 \\ 0.25 & 0 & 0.25 & 0 & 0 & 0.25 \end{bmatrix} \begin{Bmatrix} \alpha_1 \\ \alpha_2 \\ \alpha_3 \\ \alpha_4 \\ \alpha_5 \\ \alpha_6 \end{Bmatrix} \quad (3)$$

Solving Eq. (3) for unknown  $\{\alpha\}$

$$\begin{Bmatrix} \alpha_1 \\ \alpha_2 \\ \alpha_3 \\ \alpha_4 \\ \alpha_5 \\ \alpha_6 \end{Bmatrix} = \begin{bmatrix} 1 & 0 & 0 & 0 & 0 & 0 \\ 0 & 1 & 0 & 0 & 0 & 0 \\ 0 & 0 & 1 & 0 & 0 & 0 \\ -1 & -1 & 0 & 4 & 0 & 0 \\ 0 & -1 & -1 & 0 & 4 & 0 \\ -1 & 0 & -1 & 0 & 0 & 4 \end{bmatrix} \begin{Bmatrix} u_1 \\ u_2 \\ u_3 \\ u_4 \\ u_5 \\ u_6 \end{Bmatrix} \quad (4)$$

Substituting Eq. (4) into relation for displacements defined in Eq. (2)

$$u = [L_1^2 \ L_2^2 \ L_3^2 \ L_1 L_2 \ L_2 L_3 \ L_3 L_1] \begin{bmatrix} 1 & 0 & 0 & 0 & 0 & 0 \\ 0 & 1 & 0 & 0 & 0 & 0 \\ 0 & 0 & 1 & 0 & 0 & 0 \\ -1 & -1 & 0 & 4 & 0 & 0 \\ 0 & -1 & -1 & 0 & 4 & 0 \\ -1 & 0 & -1 & 0 & 0 & 4 \end{bmatrix} \begin{Bmatrix} u_1 \\ u_2 \\ u_3 \\ u_4 \\ u_5 \\ u_6 \end{Bmatrix}$$

or

$$u = [L_1(2L_1 - 1) \ L_2(2L_2 - 1) \ L_3(2L_3 - 1) \ 4L_1 L_2 \ 4L_2 L_3 \ 4L_3 L_1] \{u\}_e \quad (5a)$$

where

$$\{u\}_e^T = [u_1 \ u_2 \ u_3 \ u_4 \ u_5 \ u_6] \quad (5b)$$

Eq. (5 (a)) can be expressed as

$$\begin{aligned} u &= [M_1 \ M_2 \ M_3 \ M_4 \ M_5 \ M_6] \{u\}_e \\ M_1 &= L_1(2L_1 - 1); \ M_2 = L_2(2L_2 - 1); \ M_3 = L_3(2L_3 - 1) \\ M_4 &= 4L_1L_2; \ M_5 = 4L_2L_3; \ M_6 = 4L_3L_1 \end{aligned} \quad (6)$$

$M_1$  to  $M_6$  are the components of the shape function defined in a triangular  $XZ$  plane. Similarly the quadratic variation of displacements in a three node line with length  $2L_y$  along  $Y$ -axis can be expressed by

$$\begin{aligned} v &= \beta_1 + \beta_2 y + \beta_3 y^2 = [1 \ y \ y^2] \{\beta\} \\ \{\beta\}^T &= [\beta_1 \ \beta_2 \ \beta_3] \end{aligned} \quad (7)$$

From geometry of the element (Fig. 2)

$$\begin{Bmatrix} v_1 \\ v_2 \\ v_3 \end{Bmatrix} = \begin{bmatrix} 1 & -L_y & L_y^2 \\ 1 & 0 & 0 \\ 1 & L_y & L_y^2 \end{bmatrix} \begin{Bmatrix} \beta_1 \\ \beta_2 \\ \beta_3 \end{Bmatrix} \quad (8)$$

Solving Eq. (8) for unknown  $\{\beta\}$

$$\begin{Bmatrix} \beta_1 \\ \beta_2 \\ \beta_3 \end{Bmatrix} = \begin{bmatrix} 0 & 1 & 0 \\ -0.5/L_y & 0 & 0.5/L_y \\ 0.5/L_y^2 & -1/L_y^2 & 0.5/L_y^2 \end{bmatrix} \begin{Bmatrix} v_1 \\ v_2 \\ v_3 \end{Bmatrix} \quad (9)$$

Substituting Eq. (9) into Eq. (7)

$$v = [1 \ y \ y^2] \begin{bmatrix} 0 & 1 & 0 \\ -0.5/L_y & 0 & 0.5/L_y \\ 0.5/L_y^2 & -1/L_y^2 & 0.5/L_y^2 \end{bmatrix} \begin{Bmatrix} v_1 \\ v_2 \\ v_3 \end{Bmatrix}$$

or

$$v = [-0.5(y/L_y - y^2/L_y^2) \ (1 - y^2/L_y^2) \ 0.5(y/L_y + y^2/L_y^2)] \{v\}_e$$

or

$$v = [-0.5(\eta - \eta^2) \quad (1 - \eta^2) \quad 0.5(\eta + \eta^2)]\{v\}_e; \quad \eta = y/L_y \quad (10)$$

Combining quadratic variation of displacements in  $XZ$  plane and  $Y$ -direction, the displacements can be expressed by shape functions as follows.

$$u = \sum_{i=1}^{18} N_i u_i; \quad v = \sum_{i=1}^{18} N_i v_i; \quad w = \sum_{i=1}^{18} N_i w_i \quad (11)$$

where

$$N_i = M_j f_k(\eta); \quad j = 1, 6; \quad k = 1, 3 \quad \text{and} \quad i = 6(k-1) + j$$

$$f_1(\eta) = -0.5\eta(1-\eta); \quad f_2(\eta) = 1-\eta^2; \quad f_3(\eta) = 0.5\eta(1+\eta) \quad (12)$$

In Eq. (12), the functions  $f_1(\eta)$  to  $f_3(\eta)$  define the variables in  $Y$ -direction, where  $\eta$  is a local coordinate for the element along  $Y$  direction.

### 3.3 Element stresses and strains

The relation between strains and nodal displacements is expressed as

$$\{\varepsilon\}_e = [\varepsilon_x \quad \varepsilon_y \quad \varepsilon_z \quad \gamma_{xy} \quad \gamma_{yz} \quad \gamma_{zx}]^T$$

$$\{\varepsilon\}_e = \left[ \frac{\partial u}{\partial x} \quad \frac{\partial v}{\partial y} \quad \frac{\partial w}{\partial z} \quad \frac{\partial v}{\partial x} + \frac{\partial u}{\partial y} \quad \frac{\partial w}{\partial y} + \frac{\partial v}{\partial z} \quad \frac{\partial u}{\partial z} + \frac{\partial w}{\partial x} \right]^T$$

$$\{\varepsilon\}_e = [B]\{\delta\}_e \quad (13)$$

where  $\{\varepsilon\}_e$  is the strain vector,  $\{\delta\}_e$  is the vector of nodal displacements, and  $[B]$  is the strain displacement transformation matrix. It is further simplified as

$$[B] = [B_1 \quad B_2 \quad \cdots \quad B_i \quad \cdots \quad B_{18}] \quad (14)$$

$[B_i]$  is the strain displacement transformation sub-matrix related to displacement of node  $i$ .

$$[B_i] = \begin{bmatrix} N_i^x & 0 & 0 \\ 0 & N_i^y & 0 \\ 0 & 0 & N_i^z \\ N_i^y & N_i^x & 0 \\ 0 & N_i^z & N_i^y \\ N_i^z & 0 & N_i^x \end{bmatrix} \quad (15)$$

$[N_i^x, N_i^y, N_i^z]$  represents derivative of shape function  $N_i$  where superscript indicates derivative direction. The stresses and strains are related through elasticity constants,  $\lambda = E\mu/(1-2\mu)(1+\mu)$  and  $G = 0.5E/(1+\mu)$ , where  $\lambda$  is Lamé's constant,  $E$  is modulus of elasticity,  $\mu$  is Poisson's ratio and  $G$  is

shear modulus. The stress-strain relation is given by

$$\{\sigma\}_e = [D_c]\{\varepsilon\}_e \quad (16)$$

where  $\{\sigma\}_e$  is the stress vector, and  $[D_c]$  is the constitutive relation matrix given as

$$[D_c] = \begin{bmatrix} \lambda + 2G & \lambda & \lambda & 0 & 0 & 0 \\ \lambda & \lambda + 2G & \lambda & 0 & 0 & 0 \\ \lambda & \lambda & \lambda + 2G & 0 & 0 & 0 \\ 0 & 0 & 0 & G & 0 & 0 \\ 0 & 0 & 0 & 0 & G & 0 \\ 0 & 0 & 0 & 0 & 0 & G \end{bmatrix} \quad (17)$$

### 3.4 Element stiffness matrix and load vector

Element stiffness matrix  $[K]_e$  and load vector  $\{Q\}_e$  can be derived by using the principle of stationary potential energy. Total potential energy  $\Pi$  for an element is expressed by

$$\Pi = \frac{1}{2} \int_V \{\varepsilon\}^T \{\sigma\} dv - \int_V \{\delta\}^T \{X\} dv - \int_A \{\delta\}^T \{p\} dA \quad (18)$$

where  $\{X\}$  is the vector of body forces per unit volume,  $\{p\}$ , is the vector of surface tractions over area  $A$ ,  $\{\delta\}^T = [u \ v \ w]$  and  $\{\delta\} = [N] \{\delta\}_e$ .

Using the relations for  $\{\delta\}$ ,  $\{e\}$ , and  $\{\sigma\}$  potential energy  $\Pi$  is given as

$$\Pi = \frac{1}{2} \int_V \{\delta\}_e^T [B]^T [D_c] \{\delta\}_e dv - \int_V \{\delta\}_e^T [N]^T \{X\} dv - \int_A \{\delta\}_e^T [N]^T \{p\} dA \quad (19)$$

According to the principle of stationary potential energy, the first variation of  $\Pi$  must be zero for equilibrium condition. Taking the first variation

$$\partial \Pi = \{\partial \delta\}_e^T \left( \int_V [B]^T [D_c] dv \{\delta\}_e - \int_V [N]^T \{X\} dv - \int_A [N]^T \{p\} dA \right) = 0 \quad (20)$$

Since Eq. (20) should hold good for any variation of  $\{\partial \delta\}$

$$\int_V [B]^T [D_c] dv \{\delta\}_e - \int_V [N]^T \{X\} dv - \int_A [N]^T \{p\} dA = 0 \quad (21)$$

or

$$[K]_e \{\delta\}_e = \{Q\}_e \quad (22)$$

where

$$[K]_e = \int_V [B]^T [D_c] [B] dV \quad (23a)$$

$$\{Q\}_e = \int_V [N]^T \{X\} dV + \int_A [N]^T \{p\} dA \quad (23b)$$

are the element stiffness matrix and nodal load vector, respectively.

Eq. (23 (a)) is further expressed as

$$[K]_e = \int_V \begin{bmatrix} B_1^T \\ B_2^T \\ \vdots \\ B_i^T \\ \vdots \\ B_{18}^T \end{bmatrix} [D_c] [B_1 \ B_2 \ \cdots \ B_i \ \cdots \ B_{18}] dV \quad (24)$$

or

$$[K]_e = \begin{bmatrix} [K]_{11} & [K]_{12} & \cdots & [K]_{1i} & \cdots & [K]_{1,18} \\ [K]_{21} & [K]_{22} & \cdots & [K]_{2i} & \cdots & [K]_{2,18} \\ \vdots & \vdots & \vdots & \vdots & \vdots & \vdots \\ [K]_{i1} & [K]_{i2} & \cdots & [K]_{ii} & \cdots & [K]_{i,18} \\ \vdots & \vdots & \vdots & \vdots & \vdots & \vdots \\ [K]_{18,1} & [K]_{18,2} & & [K]_{18,i} & & [K]_{18,18} \end{bmatrix} \quad (25)$$

The details of integration procedure for individual sub-matrix  $[k]_{ij}$  are outlined in the Appendix.

The lateral force  $F_x$ , acting on the pile top, is considered as a uniformly distributed force on the top surface of the pile with intensity  $q = F_x/D^2$ . Equivalent nodal force vector,  $\{Q\}_e$ , is then expressed as

$$\{Q\}_e = \int_A q [N]^T dA \quad (26)$$

where  $[N]$  represents matrix of shape functions.

### 3.5 Assembly and solutions of equations

The element stiffness matrix  $[K]_e$  and the nodal force vector  $\{Q\}_e$ , are evaluated analytically. The 3D finite element program based on the formulation developed here is coded in the FORTRAN90 programming language, in which, the element stiffness matrix  $[K]_e$  for each element is assembled into global stiffness matrix in the skyline storage form. Similarly, the nodal load vectors are assembled into the global load vector. Algorithm for setup of assembly in skyline storage form is illustrated in Fig. 3. The system of simultaneous equations is solved for the unknown nodal displacements using active column solver. The corresponding algorithm for the active column profile symmetric equation solver is described in Fig. 4.

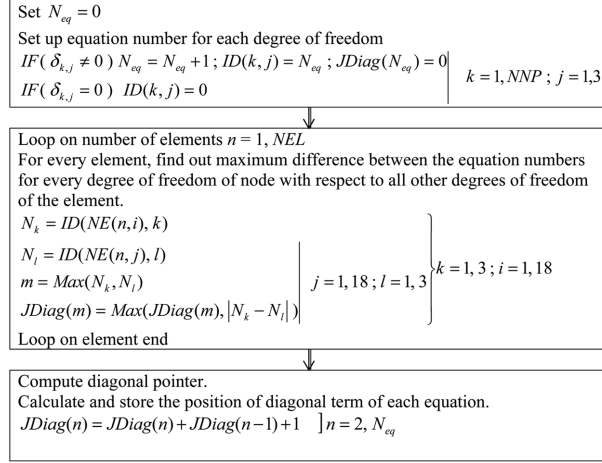


Fig. 3 Algorithm for setup of assembly in skyline storage form

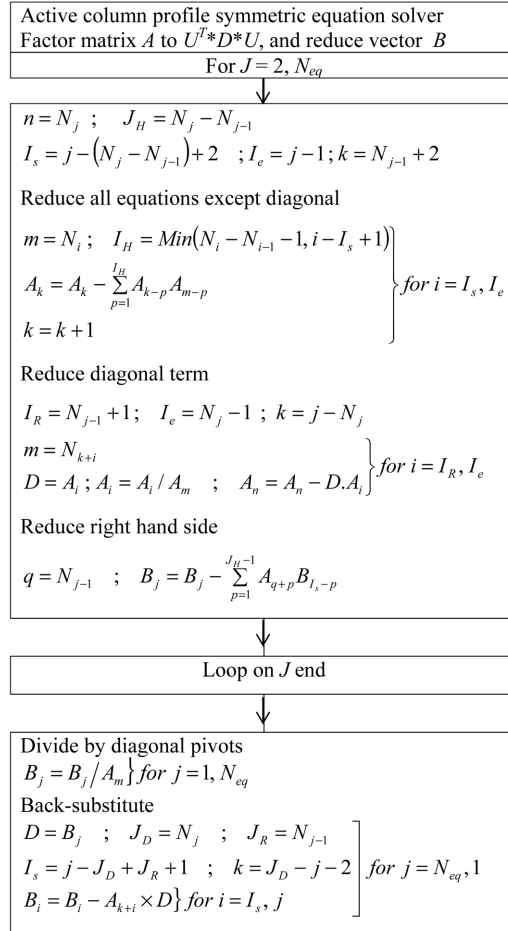


Fig. 4 Algorithm for active column solver

#### 4. Numerical analysis

The developed formulation as described in the previous sections is applied for two cases of piles in sloping ground. The width of pile is taken as 0.6 m. The  $L/D$  ratio is considered as 10. The modulus of elasticity  $E$  for pile is taken as  $2 \times 10^7$  kPa. The modulus of elasticity  $E_s$  for soil is taken as 10000 kPa for soft clay to 40000 kPa for medium clay (Das 1999). The Poisson's ratio for pile and soil are taken as 0.3 and 0.45, respectively. The edge distance  $S$  is varied as 0 and  $5D$  to examine the effect of edge distance. The ground slope is defined in terms of 1 vertical unit to  $n$  horizontal unit ( $1:n$ ). To investigate the effect of ground slope, three variations in ground slope are considered with  $n = 2, 1.5,$  and  $1$ .

Fig. 5 shows the typical variation in the displacement of the pile along its depth for  $L/D = 10$ ,  $E_s = 10000$  kPa, edge distance  $S = 0$  and ground slope  $n = 2, 1.5,$  and  $1$ . It should be noted that  $S = 0$  refers to the pile on the verge of slope (one side slope and other side level ground). The results show that for level ground case, the displacement of the pile is zero at about 4.8 m ( $8D$ ), and beyond this depth displacements are opposite to the lateral load direction, and they are small. It is noticed that at any depth, displacement of the pile is larger for greater slope. This increase in the displacement may be attributed to lesser passive resistance available for the sloping ground. A variation in the displacement of the pile along its depth is also presented for  $S = 5D$ ,  $L/D = 10$ ,  $E_s = 10000$  kPa and ground slope  $n = 2, 1.5,$  and  $1$  in Fig. 6. The trend of variation of the displacement is similar to the case of  $S = 0$  but increase in the displacements is marginal with an increase in ground slope.

The typical variation in bending moment along the pile length is presented in Fig. 7 for  $L/D = 10$ ,  $E_s = 10000$  kPa,  $S = 0$  and  $n = 2, 1.5,$  and  $1$ . It is observed that bending moments in the pile are large in the upper half of the pile. It is noticed that at any depth, bending moments in the pile is larger for greater slope. The maximum bending moment occurs at the depth of 2.1 m ( $3.5D$ ). It

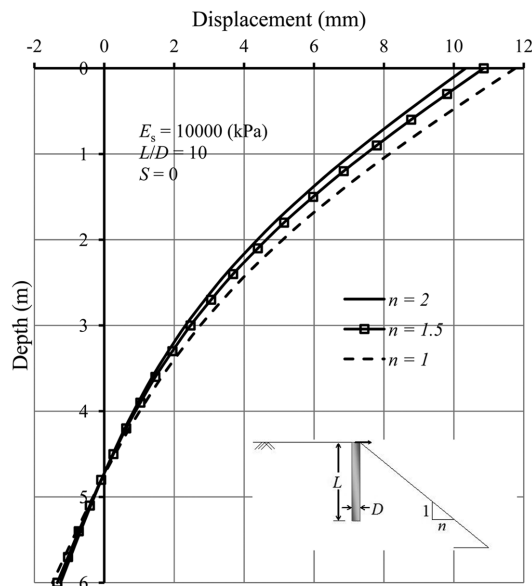


Fig. 5 Displacement pattern along the pile length ( $S = 0$ )

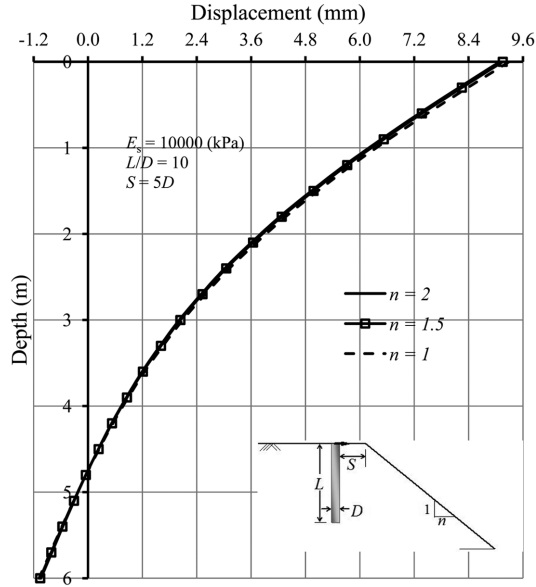


Fig. 6 Displacement pattern along the pile length ( $S = 5D$ )

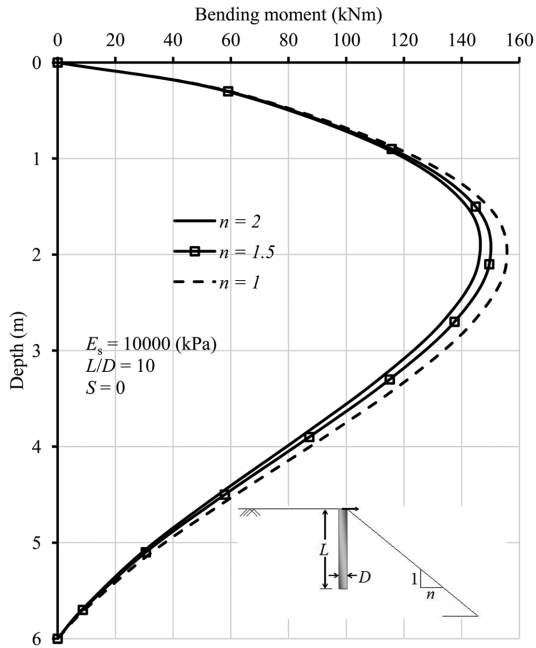


Fig. 7 Variation in bending moment along the depth of pile ( $S = 0$ )

appears that the presence of the lower passive resistance on the sloping side results in the more bending in the pile. As a result, the bending moment is higher with an increase in the ground slope. A similar trend of variation is also reported by Begum and Muthukkumaran (2008). A variation in the bending moment of the pile along its depth is also presented for  $S = 5D$ ,  $L/D = 10$ ,  $E_s = 10000$

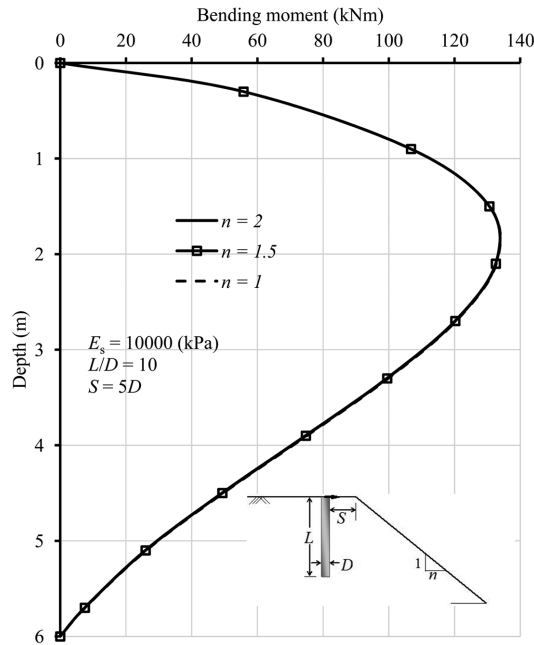


Fig. 8 Variation in bending moment along the depth of pile ( $S = 5D$ )

kPa and ground slope  $n = 2, 1.5,$  and  $1$  in Fig. 8. The trend of variation of the bending moment is similar to the case of  $S = 0$  but increase in the moments is negligible with an increase in ground slope.

The pile top displacements and the maximum bending moments are computed for various configurations considered in the present study, and are summarised in Tables 1 and 2. These values are normalised in the form of displacement ratio and moment ratio by dividing them with corresponding response at level ground ( $n = \infty$ ). For pile at crest, the change in ground slope from  $n = 2$  to  $n = 1.5$  causes an increase in the pile top displacement by around 5%, whereas a change in ground slope from  $n = 2$  to  $n = 1$  causes an increase in the pile top displacement by around 14%. The corresponding increase in the maximum moments is of the order of 3% and 7%, respectively. From displacement ratios, it is observed that displacements are increased by nearly 35% with

Table 1. Summary of pile top displacements (mm) and displacement ratio

$E_s$ (kPa)	Pile top displacements (mm)			Displacement ratio		
	$n = 2$	$n = 1.5$	$n = 1$	$n = 2$	$n = 1.5$	$n = 1$
Pile at crest						
10000	10.34	10.85	11.76	1.183	1.242	1.346
40000	3.19	3.36	3.65	1.182	1.245	1.353
Pile at $S = 5D$ from crest						
10000	9.09	9.15	9.29	1.040	1.047	1.063
40000	2.77	2.78	2.82	1.027	1.031	1.045

Table 2. Summary of maximum bending moment (kNm) and moment ratio in pile

$E_s$ (kPa)	Maximum bending moment (kNm)			Moment ratio		
	$n = 2$	$n = 1.5$	$n = 1$	$n = 2$	$n = 1.5$	$n = 1$
Pile at crest						
10000	145.70	149.56	155.43	1.085	1.113	1.157
40000	97.98	100.88	105.30	1.128	1.161	1.212
Pile at $S = 5D$ from crest						
10000	132.51	132.56	132.70	0.986	0.987	0.988
40000	88.17	88.16	88.16	1.015	1.015	1.015

respect to level ground condition for  $n = 1$ , which is reduced to 18% for  $n = 2$ . Similar comparison of moment ratio indicates increase of the order of 15-20% for  $n = 1$ , which is reduced to 8-12% for  $n = 2$ . It can be concluded that passive resistance available for the sloping ground increases with reduction in slope (from  $n = 2$  to  $n = 1$ ).

For pile at edge distance  $S = 5D$ , the maximum increase in the displacement is of the order of 2% with change in ground slope from  $n = 2$  to  $n = 1$ . The comparison with level ground response indicate maximum increase in top displacement of 6.3% for  $n = 1$ , which is reduced to 4% for  $n = 2$ . As compared to the response for pile at crest, the response for pile at edge distance  $S = 5D$  have shown less increase in displacement and moments with respect to level ground as a result of more passive resistance available with increase in edge distance.

## 5. Conclusions

In the present investigation, a computer program based on a three-dimensional finite element analysis is developed to evaluate the response of laterally loaded piles embedded in sloping ground. The pile and soil system is idealized as an assemblage of 18 node triangular prism continuum elements. These elements are suitable for modelling the ground slope as well as the response of a system dominated by bending deformations. The developed formulation can be easily adapted to suit specific field conditions as per the requirements of the site. Developed formulation is applied for two cases of piles in sloping ground. It is noticed that at any depth, displacement of the pile is larger for greater slope. For pile at crest, the change in ground slope from 1V:2H to 1V:1H causes increase in the pile top displacement by around 14%, whereas the maximum moments are increased by 7%. The effect of sloping ground is observed to be reduced for pile at edge distance  $S = 5D$ , where the maximum increase in the displacement is of the order of 2%.

## Acknowledgements

The first author wishes to express his sincere thanks to the Australian Government, Department of Education, Employment and Workplace Relations (DEEWR) for financial support through the Endeavour Award scheme.

## References

- Ashour, M., Norris, G.M. and Pilling, P. (1998), "Laterally loading of a pile in layered soil using the strain wedge model", *J. Geotech. Geoenviron.*, **124**(4), 303-315.
- Basu, D., Salgado, R. and Prezz, M. (2009), "A continuum-based model for analysis of laterally loaded piles in layered soils", *Geotechnique*, **59**(2), 127-140.
- Begum, N.A. and Muthukkumaran, K. (2008), "Numerical modeling for laterally loaded piles on a sloping ground", *Proceedings of the 12th International Conference of International Association for Computer Methods and Advances in Geomechanics, (IACMAG)*, Goa, India, 1-6 October, 2008.
- Brown, D. A. and Shie, C.F. (1991), "Some numerical experiments with a three-dimensional finite element model of a laterally loaded pile", *Comput. Geotech.*, **12**, 149-162
- Budhu M., and Davies, T. G. (1988), "Analysis of laterally loaded piles in soft clays", *J.Geotech.Eng.*, **114**(1), 21-39.
- Chae, K.S., Ugai, K. and Wakai, A. (2004), "Lateral resistance of short single piles and pile groups located near slopes", *Int. J.Geomech.*, **4**(2), 93-103.
- Charles, W.W., Ng and Zhang, L.M. (2001), "Three-dimensional analysis of performance of laterally loaded sleeved piles in sloping ground", *J. Geotech. Geoenviron.*, **127**(6), 499-509
- Das, B.M. (1999), *Principles of Foundation Engineering*, Ed. 4th, PWS Publishing, Pacific Grove, CA.
- Davisson, M.T. and Gill, H.L. (1963) "Laterally loaded piles in a layered soil system", *J. Soil Mech. Found. Div.*, **89**(3), 63-94.
- Desai, C.S. and Appel, G.C. (1976), "3-D analysis of laterally loaded structures", *Proceedings of the 2nd International Conference on Numerical Methods in Geomechanics*, Blacksburg.
- Dewaikar, D.M., Chore, H.S., Goel, M.D. and Mutgi, P.R. (2011), "Lateral resistance of long piles in cohesive soils using p-y curves", *J. Struct. Eng. - SERC*, **38**(3), 2011, 222-227.
- Fan, C.C. and Long, J.H. (2005), "Assessment of existing methods for predicting soil response of laterally loaded piles in sand", *Comput. Geotech.*, **32**(4), 274-289.
- Gabr, M.A. and Borden, R.H. (1990), "Lateral analysis of piers constructed on slopes", *J.Geotech. Eng.*, **120**(5), 816-837.
- Georgiadis, K. and Georgiadis, M. (2010), "Undrained lateral pile response in sloping ground", *J. Geotech. Geoenviron.*, **136**(11), 1489-1500.
- Matlock, H. (1970), "Correlations for design of laterally loaded piles in soft clay", *Proceedings of the 2nd Offshore Technology Conf.*, Houston.
- Matlock, H. and Reese, L.C. (1960), "Generalized solutions for laterally loaded piles", *J.Soil Mech.Found.*, **86**(5), 63-91.
- Martin, G.R. and Chen, C.Y. (2005), Response of piles due to lateral slope movement, *Comput. Struct.*, **83**, 588-598.
- Mezazigh, S. and Levacher, D. (1998), "Laterally loaded piles in sand: Slope effect on p-y reaction curves", *Can. Geotech. J.*, **35**(3), 433-441.
- Muthukkumaran, K., Sundaravadivelu, R. and Gandhi, S.R. (2004), "Effect of sloping ground on single pile load deflection behaviour under lateral soil movement", *Proceedings of the 13th World Conference on Earthquake Engineering*, Vancouver, B.C., Canada, August 1-6.
- Norris, G.M. (1986), "Theoretically based BEF laterally loaded pile analysis", *Proceedings of the 3rd International Conference on Numerical Methods in Offshore Piling*, Nantes, France.
- Poulos, H.G. (1971), "Behavior of laterally loaded piles-I: Single piles", *J. Soil Mech. Found. Div.*, **97**(5), 711-731.
- Prakash, S. and Kumar, S. (1996), "Nonlinear lateral pile deflection prediction in sands", *J. Geotech. Eng.*, **122**(2), 130-138
- Randolph, M.F. (1981), "The response of flexible piles to lateral loading", *Geotechnique*, **31**(2), 247-259.
- Reese, L.C. and Matlock, H. (1956), "Non-dimensional solutions for laterally loaded piles with soil modulus assumed proportional to depth", *Proceedings of the 8th Texas Conf. on Soil Mechanics and Foundation Engineering*, Austin, Texas.
- Reese, L.C. and Welch, R.C. (1975), "Lateral loading of deep foundations in stiff clay", *J. Geotech. Eng. Div.*, **101**(7), 633-649.

- Stewart, D.P. (1999), "Reduction of undrained lateral pile capacity in clay due to an adjacent slope", *Australian Geomech.*, **34**(4), 17-23.
- Zhang, Liyang. (2009), "Nonlinear analysis of laterally loaded rigid piles in cohesionless soil", *Comput. Geotech.*, **36**, 718-724
- Zhang, L.M., McVat, M. C. and Lai, P.W. (1999), "Centrifuge modeling of laterally loaded single battered piles in sand", *Can. Geotech. J.*, **36**(6), 1074-1084.

## Appendix

Individual sub-matrix  $[k]_{ij}$  defined in Eq. (25) can be evaluated as follows.

$$[k]_{ij} = \int_V [B_i^T][D_c][B_j] dV \quad (\text{a1})$$

where

$$[B_i^T][D_c][B_j] = \begin{bmatrix} \lambda_G N_i^x N_j^x + G N_i^y N_j^y + G N_i^z N_j^z & \lambda N_i^x N_j^y + G N_i^y N_j^x & \lambda N_i^x N_j^z + G N_i^z N_j^x \\ \lambda N_i^y N_j^x + G N_i^x N_j^y & G N_i^x N_j^x + \lambda_G N_i^y N_j^y + G N_i^z N_j^z & \lambda N_i^y N_j^z + G N_i^z N_j^y \\ \lambda N_i^z N_j^x + G N_i^x N_j^z & \lambda N_i^z N_j^y + G N_i^y N_j^z & G N_i^x N_j^x + G N_i^y N_j^y + \lambda_G N_i^z N_j^z \end{bmatrix}$$

where  $\lambda_G = (\lambda + 2G)$  (a2)

The shape functions and their derivatives are further simplified using Eq. (12) for the purpose of integration as follows.

$$\begin{aligned} N_i^x N_j^x &= M_k^x f_m(\eta) M_l^x f_n(\eta) = M_k^x M_l^x f_m(\eta) f_n(\eta) \\ N_i^x N_j^y &= M_k^x f_m(\eta) M_l^y f_n(\eta) = M_k^x M_l^y f_m(\eta) f_n(\eta) \\ N_i^x N_j^z &= M_k^x f_m(\eta) M_l^z f_n(\eta) = M_k^x M_l^z f_m(\eta) f_n(\eta) \\ N_i^y N_j^x &= M_k^y f_m(\eta) M_l^x f_n(\eta) = M_k^y M_l^x f_m(\eta) f_n(\eta) \\ N_i^y N_j^y &= M_k^y f_m(\eta) M_l^y f_n(\eta) = M_k^y M_l^y f_m(\eta) f_n(\eta) \\ N_i^y N_j^z &= M_k^y f_m(\eta) M_l^z f_n(\eta) = M_k^y M_l^z f_m(\eta) f_n(\eta) \\ N_i^z N_j^x &= M_k^z f_m(\eta) M_l^x f_n(\eta) = M_k^z M_l^x f_m(\eta) f_n(\eta) \\ N_i^z N_j^y &= M_k^z f_m(\eta) M_l^y f_n(\eta) = M_k^z M_l^y f_m(\eta) f_n(\eta) \\ N_i^z N_j^z &= M_k^z f_m(\eta) M_l^z f_n(\eta) = M_k^z M_l^z f_m(\eta) f_n(\eta) \end{aligned}$$

$k, l = 1, 6; \quad m, n = 1, 3$  (a3)

From the Eq. (a3), it is necessary to integrate three terms  $(f_m(\eta)f_n(\eta), f_m(\eta)f_n^y(\eta), f_m^y(\eta)f_n^y(\eta))$ ;  $m, n = 1, 3$  over the length of the element in  $Y$ -direction, and the six terms  $M_k^x M_l^y, M_k^y M_l^x, M_k^x M_l^z, M_k^z M_l^x, M_k^y M_l^z, M_k^z M_l^y$ ;  $k, l = 1, 6$  are to be integrated over the triangular area of the element in  $XZ$  plane. Final expressions are summarized below.

$$\int_A M_i M_j dA \quad (i = 1, 6 \text{ and } j = 1, 6)$$

$$= \frac{A}{180} \begin{bmatrix} 6 & -1 & -1 & 0 & -4 & 0 \\ -1 & 6 & -1 & 0 & 0 & -4 \\ -1 & -1 & 6 & -4 & 0 & 0 \\ 0 & 0 & -4 & 32 & 16 & 16 \\ -4 & 0 & 0 & 16 & 32 & 16 \\ 0 & -4 & 0 & 16 & 16 & 32 \end{bmatrix} \quad (\text{a4})$$

$$\int_A M_i^X M_j^X dA \quad (i = 1, 6 \text{ and } j = 1, 6)$$

$$= \frac{1}{12A} \begin{bmatrix} 3b_1^2 & -b_1b_2 & -b_1b_3 & 4b_1b_2 & 0 & 4b_1b_3 \\ -b_2b_1 & 3b_2^2 & -b_2b_3 & 4b_2b_1 & 4b_2b_3 & 0 \\ -b_3b_1 & -b_3b_2 & 3b_3^2 & 0 & 4b_3b_2 & 4b_3b_1 \\ 4b_1b_2 & 4b_1b_2 & 0 & c_{44} & c_{45} & c_{46} \\ 0 & 4b_2b_3 & 4b_2b_3 & c_{54} & c_{55} & c_{56} \\ 4b_1b_3 & 0 & 4b_1b_3 & c_{64} & c_{65} & c_{66} \end{bmatrix}$$

$$c_{44} = 4b_1(2b_1 + b_2) + 4b_2(2b_2 + b_1); c_{45} = 4b_1(2b_3 + b_2) + 4b_2(b_3 + b_2); c_{46} = 4b_1(b_3 + b_1) + 4b_2(2b_3 + b_1)$$

$$c_{54} = 4b_2(b_1 + b_2) + 4b_3(2b_1 + b_2); c_{55} = 4b_2(2b_2 + b_3) + 4b_3(2b_3 + b_2); c_{56} = 4b_2(2b_1 + b_3) + 4b_3(b_1 + b_3)$$

$$c_{64} = 4b_3(2b_2 + b_1) + 4b_1(b_2 + b_1); c_{65} = 4b_3(b_2 + b_3) + 4b_1(2b_2 + b_3); c_{66} = 4b_3(2b_3 + b_1) + 4b_1(2b_1 + b_3)$$
(a5)

$$\int_A M_i M_j^X dA \quad (i = 1, 6 \text{ and } j = 1, 6)$$

$$= \frac{1}{30} \begin{bmatrix} 2b_1 & -b_2 & -b_3 & 2b_2 - b_1 & -(b_2 + b_3) & 2b_3 - b_1 \\ -b_1 & 2b_2 & -b_3 & 2b_1 - b_2 & 2b_3 - b_2 & -(b_1 + b_3) \\ -b_1 & -b_2 & 2b_3 & -(b_1 + b_2) & 2b_2 - b_3 & 2b_1 - b_3 \\ 3b_1 & 3b_2 & -b_3 & 8(b_1 + b_2) & 4(b_2 + 2b_3) & 4(b_1 + 2b_3) \\ -b_1 & 3b_2 & 3b_3 & 4(b_2 + 2b_1) & 8(b_2 + b_3) & 4(b_3 + 2b_1) \\ 3b_1 & -b_2 & 3b_3 & 4(b_1 + 2b_2) & 4(b_3 + 2b_2) & 8(b_3 + b_1) \end{bmatrix} \quad (\text{a6})$$

$$\int_A M_i M_j^Y dA \quad (i = 1, 6 \text{ and } j = 1, 6)$$

$$= \frac{1}{30} \begin{bmatrix} 2a_1 & -a_2 & -a_3 & 2a_2 - a_1 & -(a_2 + a_3) & 2a_3 - a_1 \\ -a_1 & 2a_2 & -a_3 & 2a_1 - a_2 & 2a_3 - a_2 & -(a_1 + a_3) \\ -a_1 & -a_2 & 2a_3 & -(a_1 + a_2) & 2a_2 - a_3 & 2a_1 - a_3 \\ 3a_1 & 3a_2 & -a_3 & 8(a_1 + a_2) & 4(a_2 + 2a_3) & 4(a_1 + 2a_3) \\ -a_1 & 3a_2 & 3a_3 & 4(a_2 + 2a_1) & 8(a_2 + a_3) & 4(a_3 + 2a_1) \\ 3a_1 & -a_2 & 3a_3 & 4(a_1 + 2a_2) & 4(a_3 + 2a_2) & 8(a_3 + a_1) \end{bmatrix} \quad (\text{a7})$$

$$\int_A M_i^y M_j^y dA \quad (i = 1, 6 \text{ and } j = 1, 6)$$

$$= \frac{1}{12A} \begin{bmatrix} 3a_1^2 & -a_1a_2 & -a_1a_3 & 4a_1a_2 & 0 & 4a_1a_3 \\ -a_2a_1 & 3a_2^2 & -a_2a_3 & 4a_2a_1 & 4a_2a_3 & 0 \\ -a_3a_1 & -a_3a_2 & 3a_3^2 & 0 & 4a_3a_2 & 4a_3a_1 \\ 4a_1a_2 & 4a_1a_3 & 0 & d_{44} & d_{45} & d_{46} \\ 0 & 4a_2a_3 & 4a_2a_3 & d_{54} & d_{55} & d_{56} \\ 4a_1a_3 & 0 & 4a_1a_3 & d_{64} & d_{65} & d_{66} \end{bmatrix}$$

$$d_{44} = 4a_1(2a_1 + a_2) + 4a_2(2a_2 + a_1); d_{45} = 4a_1(2a_3 + a_2) + 4a_2(a_3 + a_2); d_{46} = 4a_1(a_3 + a_1) + 4a_2(2a_3 + a_1)$$

$$d_{54} = 4a_2(a_1 + a_2) + 4a_3(2a_1 + a_2); d_{55} = 4a_2(2a_2 + a_3) + 4a_3(2a_3 + a_2); d_{56} = 4a_2(2a_1 + a_3) + 4a_3(a_1 + a_3)$$

$$d_{64} = 4a_3(2a_2 + a_1) + 4a_1(a_2 + a_1); d_{65} = 4a_3(a_2 + a_3) + 4a_1(2a_2 + a_3); d_{66} = 4a_3(2a_3 + a_1) + 4a_1(2a_1 + a_3)$$
(a8)

$$\int_A M_i^x M_j^y dA \quad (i = 1, 6 \text{ and } j = 1, 6)$$

$$= \frac{1}{12A} \begin{bmatrix} 3b_1a_1 & -b_1a_2 & -b_1a_3 & 4b_1a_2 & 0 & 4b_1a_3 \\ -b_2a_1 & 3b_2a_2 & -b_2a_3 & 4b_2a_1 & 4b_2a_3 & 0 \\ -b_3a_1 & -b_3a_2 & 3b_3a_3 & 0 & 4b_3a_2 & 4b_3a_1 \\ 4a_1b_2 & 4a_2b_1 & 0 & e_{44} & e_{45} & e_{46} \\ 0 & 4a_2b_3 & 4a_3b_2 & e_{54} & e_{55} & e_{56} \\ 4a_1b_3 & 0 & 4a_3b_1 & e_{64} & e_{65} & e_{66} \end{bmatrix}$$

$$e_{44} = 4b_1(2a_1 + a_2) + 4b_2(2a_2 + a_1); e_{45} = 4b_1(2a_3 + a_2) + 4b_2(a_3 + a_2); e_{46} = 4b_1(a_3 + a_1) + 4b_2(2a_3 + a_1)$$

$$e_{54} = 4b_2(a_1 + a_2) + 4b_3(2a_1 + a_2); e_{55} = 4b_2(2a_2 + a_3) + 4b_3(2a_3 + a_2); e_{56} = 4b_2(2a_1 + a_3) + 4b_3(a_1 + a_3)$$

$$e_{64} = 4b_3(2a_2 + a_1) + 4b_1(a_2 + a_1); e_{65} = 4b_3(a_2 + a_3) + 4b_1(2a_2 + a_3); e_{66} = 4b_3(2a_3 + a_1) + 4b_1(2a_1 + a_3)$$
(a9)

$$\int_{-1}^1 f_m(\eta) f_n(\eta) L_y d\eta \quad (m, n = 1, 3)$$

$$= \frac{L_y}{15} \begin{bmatrix} 4 & 2 & -1 \\ 2 & 16 & 2 \\ -1 & 2 & 4 \end{bmatrix} \quad \text{(a10)}$$

$$\int_{-1}^1 f_m^y(\eta) f_n^y(\eta) L_y d\eta \quad (m, n = 1, 3)$$

$$= \frac{1}{6L_y} \begin{bmatrix} 7 & -8 & 1 \\ -8 & 16 & -8 \\ 1 & -8 & 7 \end{bmatrix} \quad \text{(a11)}$$

$$\int_{-1}^1 f_m(\eta) f_n^y(\eta) L_y d\eta \quad (m, n = 1, 3)$$

$$= \frac{1}{6} \begin{bmatrix} -3 & 4 & -1 \\ -4 & 0 & 4 \\ 1 & 4 & 3 \end{bmatrix} \quad (\text{a12})$$

In Eqs. (a5) to (a12),  $A$  is the area of triangular plane and other constants are given as below.

$$\begin{aligned} a_1 &= x_3 - x_2; a_2 = x_1 - x_3; a_3 = x_2 - x_1 \\ b_1 &= z_2 - z_3; b_2 = z_3 - z_1; b_3 = z_1 - z_2 \\ L_y &= y_7 - y_1 \end{aligned} \quad (\text{a13})$$